Agricultural and Forest Meteorology 333 (2023) 109389

Contents lists available at ScienceDirect

Agricultural and Forest Meteorology

journal homepage: www.elsevier.com/locate/agrformet

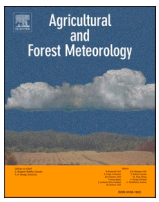

Remote sensing of seasonal variation of LAI and fAPAR in a deciduous broadleaf forest

Leticia X. Lee [a,*], Timothy G. Whitby [b], J. William Munger [b], Sophia J. Stonebrook [a], Mark A. Friedl [a]

[a] Department of Earth and Environment, Boston University, 685 Commonwealth Ave, Boston, MA 02215, United States
[b] John A. Paulson School of Engineering and Applied Sciences, Harvard University. 24 Oxford Street, Cambridge, MA 02138, United States

ARTICLE INFO

Keywords:
Leaf area index
Fraction of absorbed photosynthetically active radiation
Vegetation indices
Remote sensing
Harmonized landsat-sentinel 2
Phenology

ABSTRACT

Climate change is affecting the phenology of terrestrial ecosystems. In deciduous forests, phenology in leaf area index (LAI) is the primary driver of seasonal variation in the fraction of absorbed photosynthetically active radiation (fAPAR), which drives photosynthesis. Remote sensing has been widely used to estimate LAI and fAPAR. However, while many studies have examined both empirical and model-based relationships among LAI, fAPAR, and spectral vegetation indices (SVI) from remote sensing, few studies have systematically and empirically examined how relationships among these variables change over the growing season. In this study, we examine how and why seasonal-scale covariation differs among time series of remotely sensed SVIs and both LAI and fAPAR based on current understanding and theory. To do this we use newly available remote sensing data sets in combination with time series of in-situ measurements and a canopy radiative transfer model to analyze how seasonal variation in canopy and environmental conditions affect relationships among remotely sensed SVIs, LAI, and fAPAR at a temperate deciduous forest site in central Massachusetts. Our results show that accounting for seasonal variation in canopy shadowing, which is driven by variation in solar zenith angle, improved remote sensing-based estimates of LAI, fAPAR, and daily total APAR. Specifically, we show that the phenology of SVIs is strongly influenced by seasonal variation in near infrared (NIR) reflectance arising from systematic variation in the canopy shadow fraction that is independent of changes in LAI or fAPAR. Results of this work provide a refined basis for understanding how remote sensing can be used to monitor and model the phenology of LAI, fAPAR, APAR, and gross primary productivity in temperate deciduous forests.

1. Introduction

Climate change is affecting the growing season of terrestrial ecosystems in myriad ways (Richardson et al. 2013). One of the most widely cited examples of such impacts is changes in the length of the growing season from warming temperatures (Piao et al., 2019). These changes directly influence ecosystem-atmosphere exchanges of carbon, energy, and water budgets at seasonal time scale (Bonan & Doney, 2018). For example, a number of studies have shown that earlier leaf emergence in spring increases carbon uptake early in the growing season (Buermann et al., 2013; Keenan et al., 2014; A. D. Richardson et al., 2009, 2010), but can also reduce carbon uptake later in the growing season due to the effects of moisture limitations (Buermann et al. 2013, Wolf et al. 2015, He et al. 2020), carbon saturation (Zani et al. 2020), or nitrogen limitation (Elmore et al., 2016). Similarly, longer and warmer autumns have been shown to increase respiration and decrease net carbon uptake (D. Liu et al., 2018). Because global ecosystems are coupled to the climate system (Anav et al., 2015; Bonan & Doney, 2018; Friedlingstein, 2015; Le Quéré et al., 2018; Schimel et al., 2015), better understanding is needed regarding how changes in phenology will impact terrestrial carbon, energy, and water budgets in the future.

Seasonal variation in leaf area index (LAI) is the primary biophysical manifestation of vegetation phenology. Phenology in LAI, in combination with seasonal variation in solar geometry, drive concomitant changes in the fraction of photosynthetically active radiation absorbed by vegetation (fAPAR). Supported by theoretical results from canopy radiative transfer models (Baret & Guyot, 1991; Goward & Huemmrich, 1992; Sellers, 1985), spectral vegetation indices (SVIs) have been used for decades to monitor and map both phenology (Jonsson & Eklundh, 2002; X. Zhang et al., 2003) and variation in canopy LAI and fAPAR

* Corresponding author.
E-mail address: leticial@bu.edu (L.X. Lee).

https://doi.org/10.1016/j.agrformet.2023.109389
Received 28 September 2022; Received in revised form 17 February 2023; Accepted 19 February 2023
Available online 3 March 2023

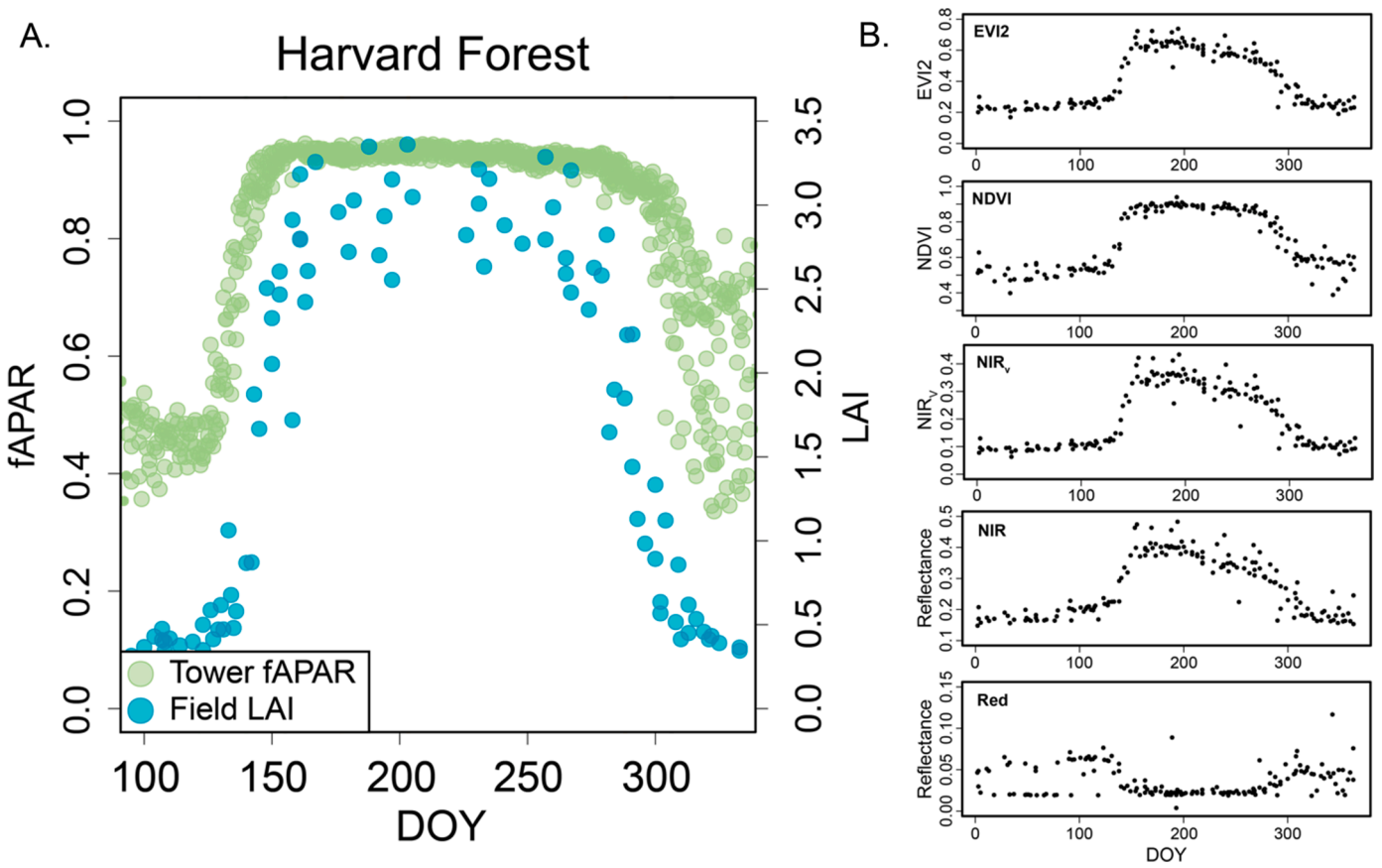

Fig. 1. (A) fAPAR and LAI measurements versus day of year at the Harvard Forest from 2016-2019. (B) SVIs (EVI2, NDVI, NIR_V) and red and near-infrared reflectance versus day of year at the Harvard Forest for HLS data from 2016-2019.

(Daughtry et al., 1982; Gitelson et al., 2003; Hipps, 1983; Penuelas et al., 1995; J. Xiao et al., 2019). In deciduous forests, seasonal variation in LAI is the primary driver of seasonal variation in fAPAR. However, additional factors that vary over the growing season, including solar geometry, moisture stress, changes in canopy chemistry and leaf orientation, and the ratio of direct to diffuse incident radiation, can influence the relationship between SVIs and fAPAR (e.g., Reaves et al. 2018). While many studies have examined both empirical and theoretical relationships among SVIs, LAI, and fAPAR (*e.g.* Asrar et al. 1984, Baret and Guyot 1991, Myneni and Williams 1994, Myneni et al. 1995, Knyazikhin et al. 1998a, 1998b, Fensholt et al. 2004, Baret et al. 2007, Yan et al. 2016a, 2016b), incomplete understanding regarding how seasonal changes in canopy properties and environmental conditions impact these relationships is a significant source of uncertainty in remotely sensed estimates of LAI and fAPAR.

With this context in mind, the goal of this paper is to use newly available remote sensing data sets in combination with time series measurements of both LAI and fPAR collected in-situ to improve understanding of how seasonal variation in canopy and environmental conditions affect the relationship between remotely sensed SVIs and LAI and fAPAR. Specifically, our analysis examines the following question: what controls changes in the relationship between remotely sensed SVI's and both LAI and fAPAR at seasonal time scale? To address this question, we use in-situ measurements and satellite imagery in combination with a canopy radiative transfer modeling framework to perform a systematic analysis of seasonal-scale co-variation between SVIs and both LAI and fAPAR at the Harvard Forest Long Term Ecological Research/AmeriFlux site in central Massachusetts.

2. Data and methods

Our analysis uses field measurements of LAI and fAPAR in combination with time series of remotely sensed surface reflectance data from the Landsat 8 Operational Land Imager and the Sentinel 2 Multispectral Instrument collected over four growing seasons. Specifically, we performed three main tasks: (1) analysis and modeling of seasonal co-variation in LAI and remotely sensed SVIs; (2) analysis and modeling of seasonal co-variation in fAPAR and remotely sensed SVIs; and (3) estimation of daily integrated APAR based on remotely sensed SVIs and diurnal variation in modeled instantaneous fAPAR.

2.1. Site description

We conducted our analysis using data collected at the Harvard Forest Long Term Ecological Research/AmeriFlux site located in Petersham, MA (https://harvardforest.fas.harvard.edu/). Species composition at the Harvard Forest is representative of a transitional New England forest, with more than 90% of the forest composed of a closed canopy dominated by red oak (*Quercus rubra),* red maple *(Acer rubrum),* yellow birch (*Betula alleghaniensis*), and Eastern Hemlock (*Tsuga canadensis*). The climate is humid continental with four distinct seasons, including warm summers (average daily July temperature of 20 C) and cold winters (average daily January temperature of -4 C). As a long-term ecological research site and an AmeriFlux core site, Harvard Forest has a long history of research and a large archive of historical data sets including eddy covariance and meteorological measurements, along with field-measured LAI and fAPAR data. The site is also a part of the National Ecological Observatory Network (NEON) network, which provides systematic monitoring of diverse ecological variables and processes that are relevant to this study, including tower-based micro-

meteorological measurements and LAI measurements.

2.2. Data

We use time series of LAI and fAPAR data collected in the footprint of the Harvard Forest Environmental Measurement Station (EMS) eddy covariance flux tower (Munger & Wofsy, 2022). in combination with time series of surface reflectance data from Landsat 8 and Sentinel 2 at 30 m spatial resolution (Fig. 1). We restrict our analyses to data collected during the growing season at Harvard Forest, which we define here as extending from April 10 to December 1 and use data from 2016-2019. Note that prior to 2016 Sentinel 2 data was acquired at roughly monthly frequency in North America. As a consequence, after cloud screening (which eliminates roughly 50% of the data during the growing season) HLS data do not provide sufficient temporal to resolve phenological processes before 2016.

Systematic LAI measurements have been collected at Harvard Forest since 2005 and are collected bi-weekly in the spring and fall and monthly during the mid-summer using LI-COR LAI2000 (and more recently LAI2200) optical LAI meters (LI-COR Biosciences, Lincoln, NE). Measurements are collected at 36 plots located along six 500 m transects extending radially in a cone facing to the west and extending outward in the footprint of the EMS tower. The plots are located inside 34 unique 30-meter Landsat and Sentinel-2 pixels (see below). The LAI measurements estimate total plant area index (PAI), which includes both woody and leaf components. To estimate LAI, which is our primary interest here, we adjust the measured PAI values using the woody fraction (W_f), which accounts for the effects of woody plant materials (branches, stems) on PAI measurements (J. M. Chen, 1996; G. Yan et al., 2019):

$$W_f = \frac{P - P_{min}}{P_{max}} \quad (1)$$

$$LAI = P \times (1 - W_f) \quad (2)$$

where P is the measured PAI, and P_{min} and P_{max} are the growing season minimum and maximum PAI, respectively. W_f changes as a function of the LAI and so exhibits seasonal variation during spring and fall (Ryu et al., 2012; Toda & Richardson, 2018). For the analyses we present below, we interpolate the periodic measurements of LAI to daily time step during the growing season using a cubic spline.

In situ fAPAR was estimated using 30- and 60-minute values (depending on the source) of above- and below-canopy measurements of photosynthetically active radiation (PAR) (400-700 nm) collected at three locations: (1) the EMS tower; (2) a walk-up tower located about 400 meters to the southwest of the EMS tower; and (3) the National Ecological Observatory Network (NEON) tower located about 240 meters to the Northeast of the walk-up tower. The walk-up and NEON towers are in the footprint of the EMS tower adjacent to the LAI transects. To ensure high-quality estimates of fAPAR, we excluded measurements under low light conditions (when total downwelling above canopy PAR was < 200 μmol m^{-2} s^{-1}) and for large solar zenith angles (outside of 7 AM to 5 PM local solar time). The resulting set of PAR measurements were used to calculate the absorbed photosynthetically active radiation (APAR, hereafter Φ) and fAPAR. As part of this procedure, 3 cases with out-of-range fAPAR values below 0 or above 1 (i.e., <0 or >1) were assumed to reflect low quality data and were removed.

To calculate Φ we assume that PAR reflected by the forest floor is negligible (Asner, 1998; D'Odorico et al., 2014; Jenkins et al., 2007; Li & Fang, 2015; Russell et al., 1989) and that Φ can be estimated using:

$$\Phi = PAR_i - PAR_{cr} - PAR_{tr} \quad (3)$$

where PAR_i is the incident downwelling PAR above the canopy, PAR_{cr} is the upwelling PAR reflected by the canopy, and PAR_{tr} is the transmitted PAR (*i.e.*, measured below the canopy). fAPAR was then estimated by dividing Φ by PAR_i. For PAR_i and PAR_{cr}, we used the average of measurements collected across all three towers at each time step. For PAR_{tr}, we used PAR sensors collected at 1 m above the ground surface at the hardwood walk up and EMS towers (Ellison & Munger, 2021; A. Richardson & Hollinger, 2019). PAR_{cr} measurements at the EMS data were available at 60-minute time steps and we linearly interpolated these data to a 30-minute time step.

Remotely sensed time series of surface reflectance and SVIs used in this analysis were derived from version 1.4 of NASA's Harmonized Landsat Sentinel-2 (HLS) dataset (https://hls.gsfc.nasa.gov/). This data set provides 'harmonized' surface reflectance values from imagery acquired by the Landsat 8 Operational Land Imager and Sentinel-2 Multispectral Sensor Instrument, where data from each instrument have been co-registered to a common 30 m grid, normalized to adjust for radiometric differences across sensors, corrected for solar and view geometry effects, and used to estimate surface reflectance imagery based on a common atmospheric radiative transfer model (for details, see Claverie et al. 2018). The HLS dataset includes all imagery collected by Landsat 8 and Sentinel 2A and 2B. For this analysis we use imagery collected between 2016-2019 from HLS tile T18TYN, which covers the Harvard Forest. Note that because Sentinel 2B was launched in 2017, HLS imagery has fewer images in 2016 than in 2017-2019. Because LAI and fAPAR vary at seasonal time scale (i.e., not daily) and we are interested in daily estimates of LAI and fAPAR, we interpolate the HLS to provide daily imagery using the approach described by Bolton et al. (2020) based on penalized cubic smoothing splines. Using this approach, daily values of the normalized difference vegetation index (NDVI; Tucker 1979), two-band Enhanced Vegetation Index (EVI2; Jiang et al. 2008), and near-infrared vegetation index (NIR_v; Badgley et al. 2017) for the 2016-2019 growing seasons were generated for individual HLS pixels located over each of the fixed plots where LAI measurements were collected (34 pixels, ~30,600 m^2). In the results presented below, we include values for LAI and fAPAR estimated directly from imagery and from the interpolated values of the SVIs.

2.3. Analysis

2.3.1. Estimating LAI from SVIs

In the first element of our analysis, we used the modeling framework developed by Baret and Guyot (1991) in association with measurements of NDVI, EVI2, and NIR_v derived from HLS imagery to estimate the forest canopy LAI in the EMS tower footprint at daily time step during the growing seasons of 2016-2019. In this framework, which was originally derived using the SAIL canopy radiative transfer model (Verhoef, 1984), canopy LAI is estimated as a function of remotely sensed SVI measurements using a formulation based on Beer's Law:

$$LAI = \frac{ln\left(\frac{VI_{DOY} - VI_\infty}{VI_g - VI_\infty}\right)}{-k_{VI}} \quad (4)$$

where VI_{DOY} is the vegetation index on any given day of year, VI_g is the bare ground vegetation index (*i.e.*, the VI value when no green leaves are present in the canopy), VI_∞ is the deep canopy vegetation index (the VI value for a canopy with very large LAI; here we use LAI = 10), and k_{VI} is an extinction coefficient that depends on leaf optics, the canopy leaf angle distribution, and solar geometry (see next section). Because the LAI and HLS data were not acquired on the same dates, we compared LAI values estimated from remotely sensed SVIs to field measurements of LAI interpolated to the HLS image acquisition dates.

2.3.2. Two-stream modeling of canopy reflectance

Both VI_∞ and k_{VI} depend on solar geometry and canopy conditions, and so our approach includes parameterizations that capture variation in each of these terms over the course of the growing season. For example, Fig. 1 clearly shows that even though field-measured LAI is effectively constant outside of the greenup and senescence periods, EVI2 and NIRv (and to a lesser degree, NDVI) decrease monotonically after

Fig. 2. Camera image of representative forest canopy in the Harvard Forest EMS tower footprint acquired from an unmanned aerial vehicle at 14:35 pm EDT on Oct 16, 2016. Note that even though the forest canopy is relatively uniform, shadowing from within and between crown gaps and 3-D structure is substantial.

reaching peak values around the summer solstice. This seasonal pattern has been noted in other studies (e.g., Elmore et al. 2012) and was examined in detail by Reaves et al. (2018), who concluded that about 50% of the observed seasonal variation is related to topographic effects. However, Reaves et al. (2018) were not able explain the remaining variance, nor do their results explain systematic seasonal decline in vegetation indices over relative flat sites such as the Harvard Forest. Here we use the two-stream canopy radiative transfer model described by Sellers (1985) in combination with a simple parameterization for canopy shadowing as a function of solar zenith angle to model seasonal variation in VI_{∞}. Specifically, we define canopy shadows as areas in the canopy that are not illuminated by beam irradiance. To parameterize canopy properties (including variation in leaf optics) we use measurements of leaf-level red and near-infrared reflectance for dominant tree species at Harvard Forest collected by Dillen et al. (2012), and following Raabe et al. (2015), we parameterize the canopy leaf angle distribution to be planophile (i.e., we set the parameter describing the departure from a spherical LAD in the two stream model $\chi_L = 0.5$).

2.3.3. *Modeling the Impact of Canopy Shadows on Surface Reflectance*

The two-stream approximation for radiative transfer in vegetation canopies assumes a uniform optical medium. Hence, it does not account for the effects of spatial variability and three-dimensional forest structure, especially from shadows, which affect the pixel-scale surface reflectance from forest canopies (Fig. 2). To capture the impact of seasonal changes in canopy shadowing on surface reflectance, which is measured at near-nadir view angles by Sentinel 2 and Landsat 8, we implemented a simple parameterization that quantifies how the proportion of canopy that is sunlit versus shadowed changes with solar zenith angle over the growing season. The parameterization includes two parts.

First, to model the proportion of canopy that is shaded as a result mutual shadowing by leaves within crowns ($f_{L_{sl,\mu}}$), we use the ratio of sunlit LAI at the time of satellite overpass to the sunlit LAI when the Sun is at nadir ($\mu = 1$):

$$f_{L_{sl,\mu}} = 1 - \left(\frac{L_{sl,\mu}}{L_{sl,\mu=1}}\right) \tag{5}$$

In this Eq., $L_{sl,\mu}$ is the sunlit leaf area for a given solar zenith angle (specified here using the cosine of the solar zenith angle, μ) for the date and time of interest, which is estimated using (Campbell & Norman, 1998):

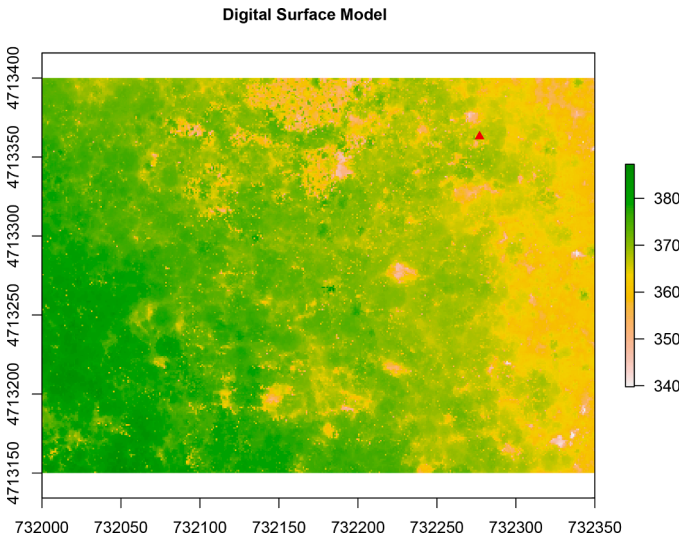

Fig. 3. NEON Digital surface model from discrete return lidar imagery for the study area where LAI and remote sensing samples were collected at the Harvard Forest. The EMS tower is identified by the red triangle in the upper right corner. Units for color scale are meters above sea level.

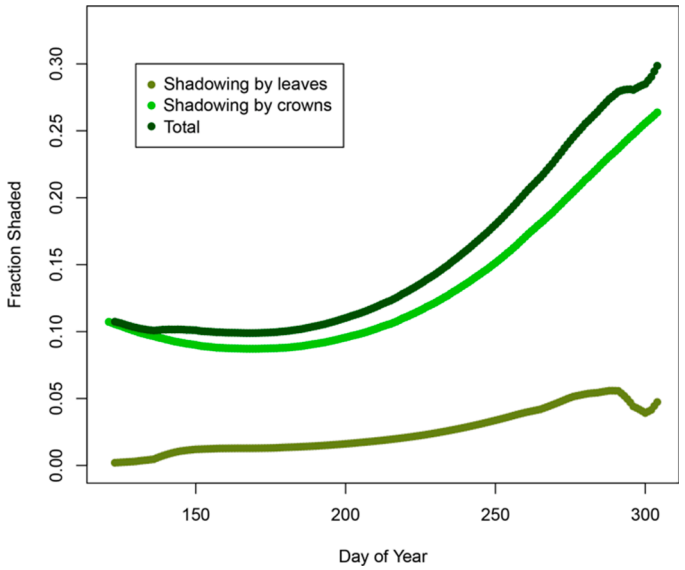

Fig. 4. Variation in shadowing in illuminated crowns by leaves within crowns ($f_{L_{sl,\mu}}$), shadowing from 3-D crown structure ($f_{sc,\mu}$), and total shadow fraction (f_{ts}) for the EMS tower footprint. Values for all three quantities are computed for solar zenith angles corresponding to the average overpass time of Landsat and Sentinel 2 each day.

$$L_{sl,\mu} = \frac{1 - e^{-K_\mu \times L}}{K_\mu} \tag{6}$$

where L is the canopy LAI for the date in question and K_μ is a shape factor that depends on μ (Sellers, 1985). Hence, $f_{L_{sl,\mu}}$ varies over the growing season as a function of both the canopy LAI (L) and μ.

Second, to estimate the proportion of the surface that is shadowed on any given date and time as a result of 3-D crown structure ($f_{sc,\mu}$) (i.e., shadowed crowns and shadows cast by 3-D crown structure), we used a high spatial resolution (1m) digital surface model (DSM) for the Harvard Forest in combination with the algorithm described by (Corripio, 2003) to model shaded versus non-shaded canopy surfaces as a function of solar zenith angle. The DSM was generated by the National Ecological

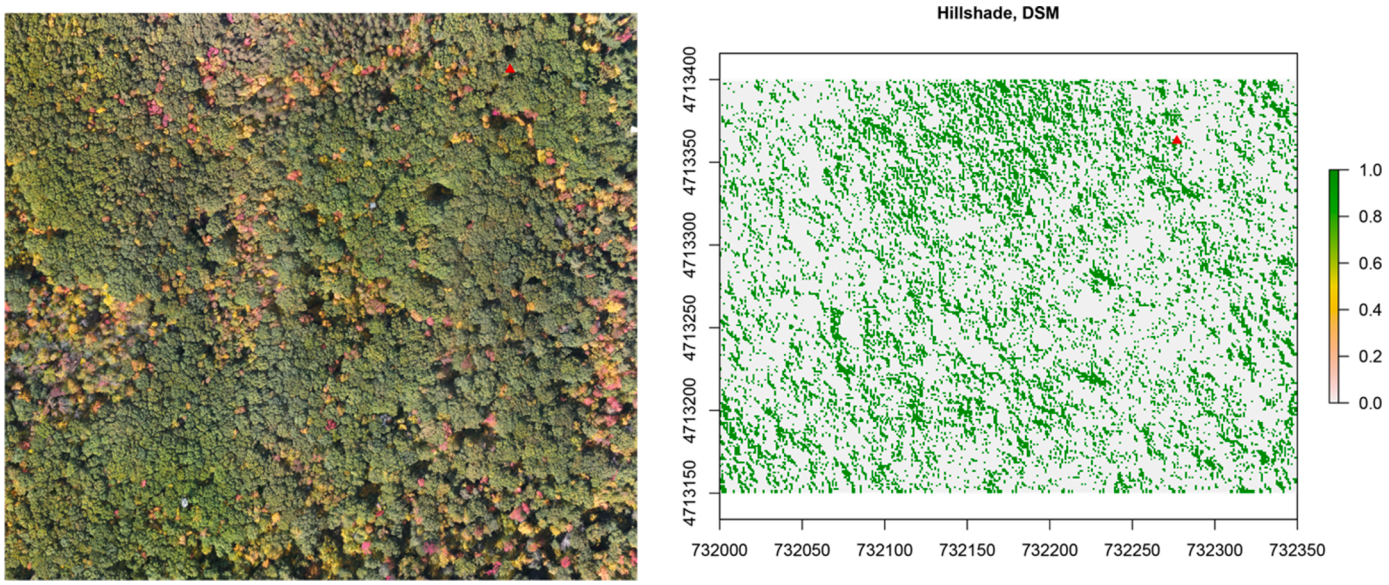

Fig. 5. Left panel: UAV image mosaic for the area corresponding to LAI plots and Landsat and Sentinel pixels used in this analysis. Right panel: shadowed (green) versus illuminated canopy mapped using NEON lidar imagery. Red triangle shows the location of the EMS tower. Note, the classification map has been reprojected to a UTM coordinate system, while the image at left is unprojected.

Observatory (NEON) using discrete return lidar imagery collected by the NEON airborne observatory at Harvard Forest (NEON data product ID DP3.30024.001), and captures high-resolution spatial variation in canopy height, including the effect of underlying topography (which is modest in the EMS footprint but can influence shadows). To estimate shade fractions for our region of interest, we extracted DSM data for the footprint of the EMS tower corresponding to the same area where the LAI and HLS data used in this study were collected (Fig. 3).

Using the DSM data, we used the 'hillshading' function implemented in Version 1.2.2 of the R package 'insol' (which implements the algorithm described in Corripio (2003)) to identify locations where the where the local solar zenith angle of 1m pixels exceeded 90° or where 3-D canopy structure resulted in shadows casted onto other 1m cells at the overpass time of Landsat and Sentinel 2 at Harvard Forest. The total shade fraction for the canopy was then computed as the sum of the fraction of shade from the crowns ($f_{sc,\mu}$) and the fraction of shade from leaves ($f_{L_{sl,\mu}}$), correcting for overlap:

$$f_{ts} = f_{sc,\mu} + \left(1 - f_{sc,\mu}\right) * f_{L_{sl,\mu}} \tag{7}$$

Fig. 4 plots seasonal variation in the modeled proportion of the total shaded area (f_{ts}) as well as the components of this shade from leaves and crowns ($f_{L_{sl,\mu}}$ and $f_{sc,\mu}$, respectively) at the nominal overpass time of Landsat and Sentinel 2. On the summer solstice (~June 21), the modeled shadow fraction is 9.9%, whereas by the end of the growing season (Oct 31) the fraction increases to 29.9%.

To evaluate the realism of model results shown in Fig. 4, we created a mosaic of high-resolution imagery collected from an unmanned aerial vehicle at the Harvard Forest and cropped the resulting image to cover the same study region that we used for the DSM-based modeling. We then manually labeled 506 pixels in this mosaic (251 as shadowed and 255 as sunlit), and used these pixels to train a random forest model (Breiman, 2001) that classifies each pixel as either sunlit or shaded. Using this classifier, we created a high-spatial resolution (10cm) map of sunlit versus shaded canopy in the study region (Fig. 5). The overall classification accuracy of the model (estimated via cross-validation) was 99.2% correctly classified and the proportion of the area mapped as shadow was 33.6%. For comparison the shade fraction modeled using Eqs. (5)-(7), is 28.1% for the date and time when the UAV imagery was acquired, which suggests that our approach modestly (~16% for the date and time the UAV imagery were acquired) underestimates shadow fraction.

2.3.4. Estimating fAPAR from In-Situ Measurements

To estimate fAPAR absorbed by leaves in the canopy ($fAPAR_C$), *in situ* measurements of total fAPAR ($fAPAR_T$) were adjusted to exclude radiation intercepted by branches and stems ($fAPAR_S$) (*i.e.*, $fAPAR_C = fAPAR_T - fAPAR_S$, where $fAPAR_T = \Phi/PAR_i$). Note that $fAPAR_S$ varies with leaf area in the canopy and so is not constant over the growing season. To account for this, we used an approach based on Beer's law to partition $fAPAR_T$ between $fAPAR_C$ and $fAPAR_S$ (Fig. 2):

$$fAPAR_C = P_\infty - exp\left(-K_\mu L\right) \tag{8}$$

$$fAPAR_S = \left(P_\infty - exp\left(-K_\mu S\right)\right) \times \left(1 - fAPAR_C\right) \tag{9}$$

where L and S are the canopy and stem area index (*i.e.*, the plant area index when LAI = 0), respectively, K_μ is the canopy extinction coefficient derived from observations, and P_∞ is the deep canopy fAPAR (=0.94).

2.3.5. Estimating fAPAR from remote sensing

We evaluate two different approaches for estimating $fAPAR_C$ from vegetation indices: (1) the method described by Baret and Guyot (1991), which estimates $fAPAR_C$ directly from SVIs; and (2) the method described by Fensholt et al. (2004), which estimates $fAPAR_C$ from canopy LAI. Because our interest is in estimating $fAPAR_C$ from remote sensing, here we evaluate this latter approach using LAI estimated from SVIs (Section 2.3.1).

The method described by Baret and Guyot (1991) (hereafter, BG91) is an extension of the approach we previously described above to estimate LAI:

$$fAPAR = P_\infty \left[1 - \left(\frac{VI_\infty - VI}{VI_\infty - VI_g}\right)^K\right] \tag{10}$$

where P_∞ is the asymptotically limiting value of fAPAR for an infinitely thick canopy (= 0.94), K is an extinction coefficient defined as the ratio between k_{VI} and K_μ at the time of satellite overpass, and VI_{DOY}, VI_g, and VI_∞ are from Eq. (4).

The method described by Fensholt et al. (2004) (hereafter FT04) uses a shape factor ($G(\theta)$, solar zenith angle (θ), and the canopy LAI to

Table 1
R^2, RMSE, and bias of LAI estimated from each vegetation index at the Harvard Forest. Note that the field LAI data were linearly interpolated between measurements to estimate in-situ LAI for HLS overpass dates.

SVI	R^2	RMSE	Bias
EVI2	0.72	0.49	0.17
NDVI	0.79	0.47	0.14
NIR_V	0.79	0.42	0.24

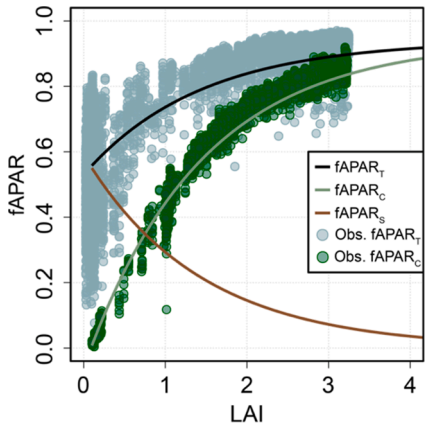

Fig. 6. Contributions of stems and leaves to total and canopy fAPAR at Harvard Forest. Lines show modeled values for mid-day conditions, and points show tower measurements, which include diurnal variation.

estimate transmittance of PAR through the canopy under clear sky conditions:

$$\mathrm{fAPAR_{tr}} = exp\left(\frac{-\mathrm{G}(\theta) \times \mathrm{L}}{cos\theta}\right) \tag{11}$$

where G(θ) is defined as:

$$\mathrm{G}(\theta) = \frac{\sqrt{x^2\cos^2\theta + \sin^2\theta}}{x + 1.774(x + 1.182) - 0.733} \tag{12}$$

and x is the ratio of the average projected area of leaves on horizontal and vertical surfaces (*e.g.*, for a spherical distribution, x is 1.0). For this study, we set x to be 3, which is consistent with χ_L in the two-stream model simulations (*i.e.*, a planophile leaf angle distribution, de Wit (1965)). $\mathrm{fAPAR_C}$ was then estimated by:

$$\mathrm{fAPAR_C} = \mathrm{P_\infty} - \mathrm{fAPAR_{tr}} \tag{13}$$

2.3.6. *Estimating daily APAR*

In the final element of our analysis, we use estimates of $\mathrm{fAPAR_C}$ derived from remote sensing to estimate daily total APAR. To do this, we model diurnal variation in fAPAR over the course of the growing season using FT04, which captures the effect of diurnal and seasonal variation in solar geometry on fAPAR, applied at 30-minute intervals between 7 AM and 5 PM local solar time from DOY 100 - 330. Then, using the downwelling incident PAR ($\mathrm{PAR_i}$) measured above the canopy at Harvard Forest, we compute daily total APAR absorbed by the canopy (Φ_D; $\mathrm{MJ/m^2/day}$) as:

$$\Phi_D = \sum_{t_0}^{t_n} \mathrm{fAPAR_C}(t) \times \mathrm{PAR}_i(t) \times 1800\ \mathrm{s} \tag{14}$$

where t is the timestep, t_0 is 7:00 AM, t_n is 5:00 PM, and $\mathrm{PAR_i}$ is the average incident PAR in the 30 minutes preceding timestep *i*.

3. Results

3.1. *Remotely sensed Estimates of LAI*

LAI values retrieved from EVI2, NDVI and NIR_V have similar accuracy, and all three vegetation indices realistically reproduce seasonal variation in LAI (Table 1, Fig. 7). More generally, the results shown in Figs. 7 and 8 and demonstrate that all three SVIs capture the overall magnitude and seasonal variation in LAI well. Note that even after careful quality control and filtering for clouds, the time series for each vegetation index includes variability that is primarily caused by noise in the NIR reflectance (Fig. 1) that propagates into retrieved LAI values.

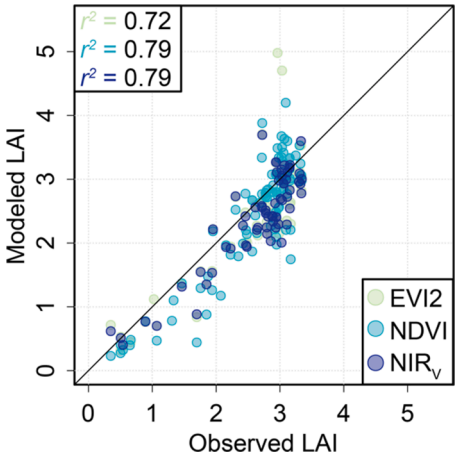

Fig. 8. LAI modeled from HLS imagery versus observed LAI from field plot data. Note that the field plot data were linearly interpolated between measurement dates to estimate in-situ LAI on HLS overpass dates. Note, this figure includes data from all four years

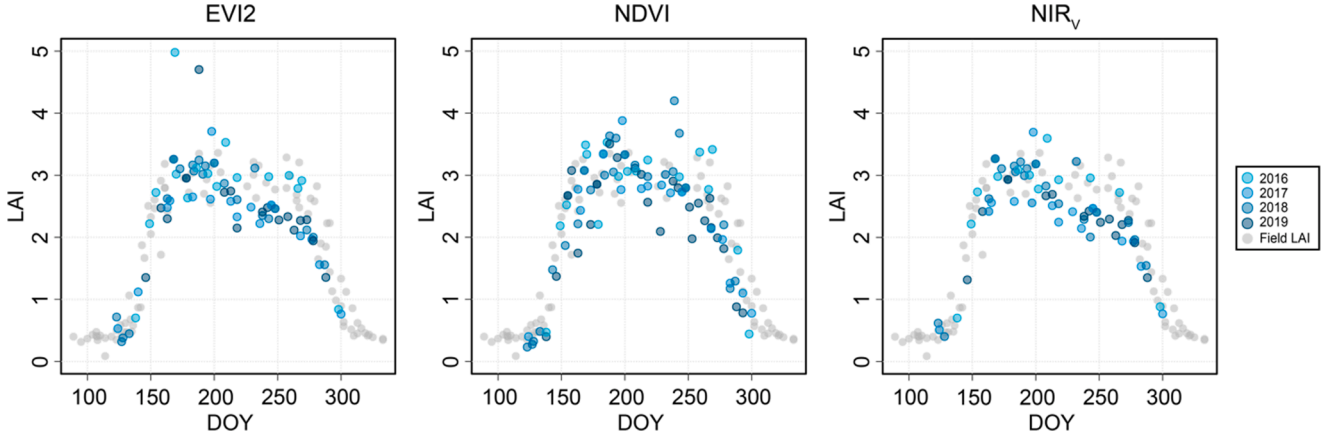

Fig. 7. Seasonal time series of LAI estimated from EVI2, NDVI, and NIR_v and field measurements at Harvard Forest.

Table 2
Agreement between field measurements of $FAPAR_C$ and corresponding values retrieved from remote sensing.

	BG91			FT04		
	R^2	RMSE	Bias	R^2	RMSE	Bias
EVI2	0.88	0.05	0.00	0.89	0.05	0.02
NDVI	0.85	0.06	0.00	0.84	0.07	0.03
NIR_V	0.85	0.05	0.00	0.87	0.05	0.03

Overall, seasonal variation in LAI estimated from each SVI follows the pattern described by Elmore et al. (2012) and Reaves et al. (2018), with maximum values around the time of the summer solstice, systematic decrease over the mid-growing season, and rapid decline in the fall related to leaf senescence and leaf drop. Fig. 7 also suggests that NDVI does a modestly better job of estimating LAI in the second half of the growing season than EVI2 or NIR_V. This reflects the fact that each of these latter two indices weight NIR reflectance more heavily than the NDVI. Hence, NDVI is less impacted by shadowing than EVI2 or NIR_V. However, results shown in Table 2 demonstrate that differences in accuracy are negligible among the three indices. Consistent with these results, Fig. 8 shows a scatterplot comparing field-measurements with remotely sensed LAI derived from each vegetation index. Significantly, results shown in Fig. 8 suggest that field-based measurements of LAI saturate at LAI values ~3.2. More generally, these results indicate that LAI estimated by all three vegetation indices tend to underestimate field

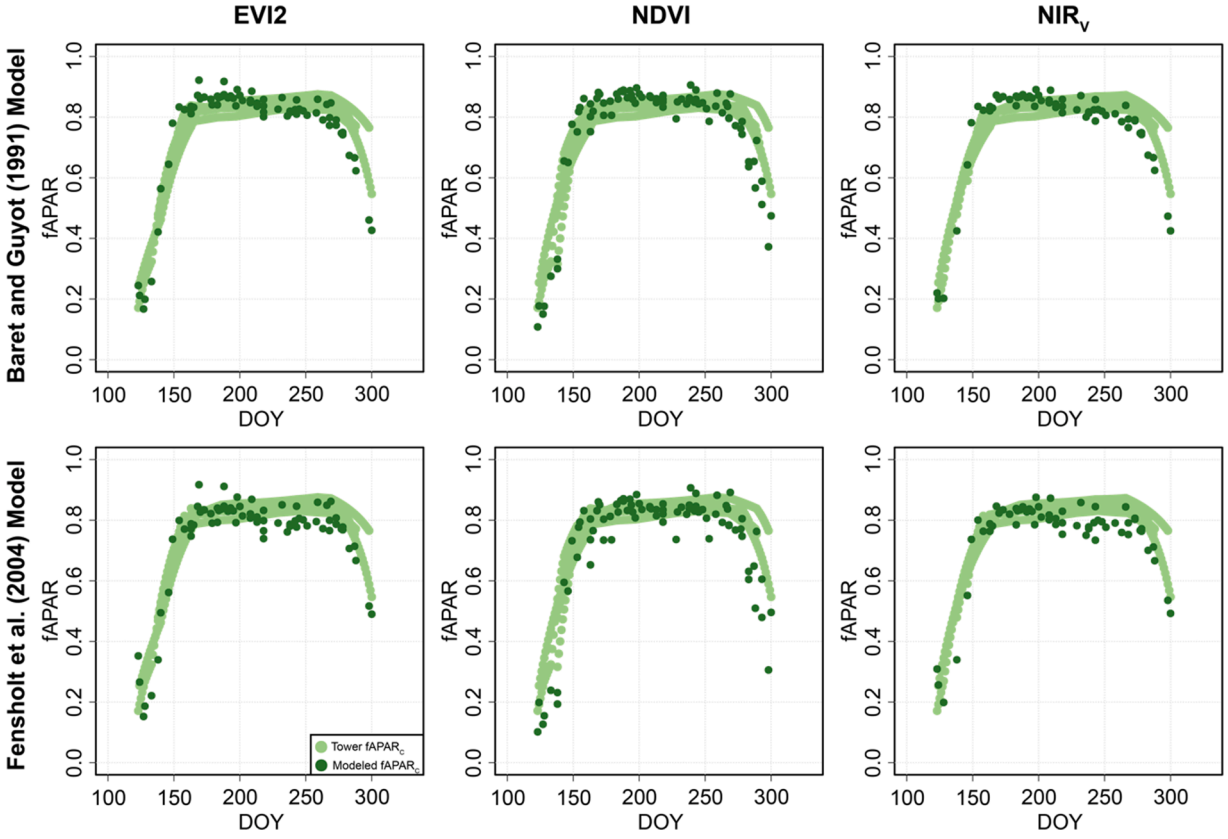

Fig. 9. Seasonal variation in observed canopy $fAPAR_C$ (i.e., from tower-based measurements) and modeled $fAPAR_C$ estimated from remote sensing using BG91 (upper row) and FT04 (lower row). Note, this figure includes data from all four years.

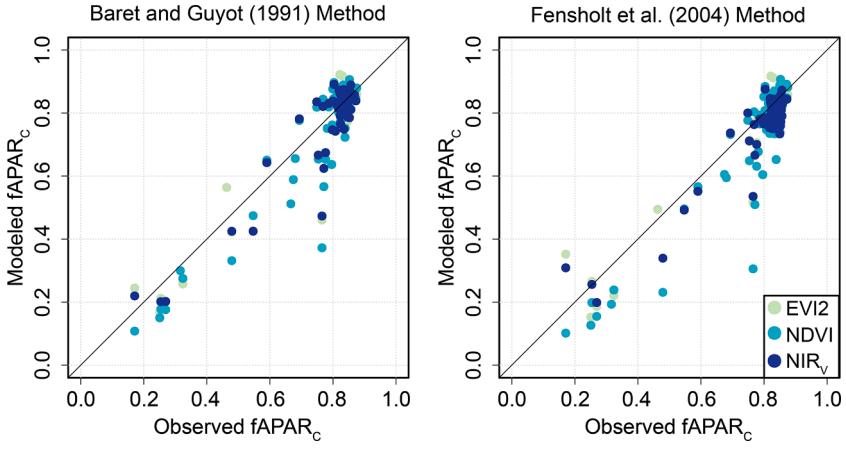

Fig. 10. Canopy $fAPAR_C$ estimated from EVI2, NDVI, and NIR_V using BG91 (left panel) and FT04 (right panel) versus observed $fAPAR_C$. Note, this figure includes data from all four years.

Table 3
Agreement between measured and modeled 30-minute canopy $fAPAR_C$ using the method described by Fensholt et al. (2004). Bias values are provided for the whole season (All), as well as for early, mid, and late season periods determined from HLS data for Harvard Forest (Bolton et al., 2020). The table shows agreement for dates when HLS imagery was acquired (HLS Acquisition Dates) and for all dates based on LAI estimated from daily interpolated SVI values (Observed + Interpolated SVI).

	HLS Acquisition Dates						Observed + Interpolated SVI					
	R^2	RMSE	Bias (All)	Bias (Early)	Bias (Mid)	Bias (Late)	R^2	RMSE	Bias (All)	Bias (Early)	Bias (Mid)	Bias (Late)
EVI2	0.91	0.07	-0.04	-0.04	-0.06	-0.01	0.94	0.06	-0.02	-0.03	-0.02	-0.01
NDVI	0.88	0.07	0.02	0.03	-0.03	0.04	0.92	0.06	0.01	0.03	-0.01	0.04
NIR_V	0.89	0.06	-0.01	0.00	-0.05	-0.02	0.92	0.05	-0.01	0.00	-0.01	-0.02

measurements of LAI throughout much of the growing season.

3.2. Remotely sensed estimates of fAPAR

Both methods that we tested to estimate $fAPAR_C$ performed well for all vegetation indices, with a few subtle differences (Figs. 9 and 10, Tables 2 and 3). Overall agreement between field measurements of $fAPAR_C$ and $fAPAR_C$ retrieved from HLS using BG91 or FT04 was high for all three SVIs, which suggests that either method can be used to estimate daily $fAPAR_C$ with good accuracy. Note that these results show $fAPAR_C$ estimated at the time of the satellite overpass (nominally, between 10:00 and 10:15 am local time), with a large majority of data points collected during the June-September period with maximum leaf area (*cf.*, Fig. 7). Retrieved $fAPAR_C$ values estimated using both methods modestly underestimate field measurements during the spring greenup and fall greendown periods when LAI is $< \sim 2$ (i.e., when fAPAR $< \sim 0.8$) (Fig. 10).

Based on the results shown in Table 2 and Fig. 5 and leveraging the fact that FT04 includes the effect of solar zenith angle on fAPAR, we used FT04 in combination with remotely sensed estimates of LAI interpolated to daily values to estimate $fAPAR_C$ at 30-minute time steps for all days during the growing seasons of 2016-2019 (Fig. 11). Results based on all three SVIs showed the same general pattern, with high agreement and low bias between modeled and observed values of $fAPAR_C$.

3.3. Estimating daily APAR

Daily absorbed photosynthetically active radiation by the canopy (Φ_D) computed from 30-minute measurements of PAR_i and modeled $fAPAR_C$ values showed strong agreement with in-situ measurements (Fig. 12 and Table 4). Anomalously high Φ_D values are the by-product of noise in the SVI observations (specifically, in the NIR measurements on

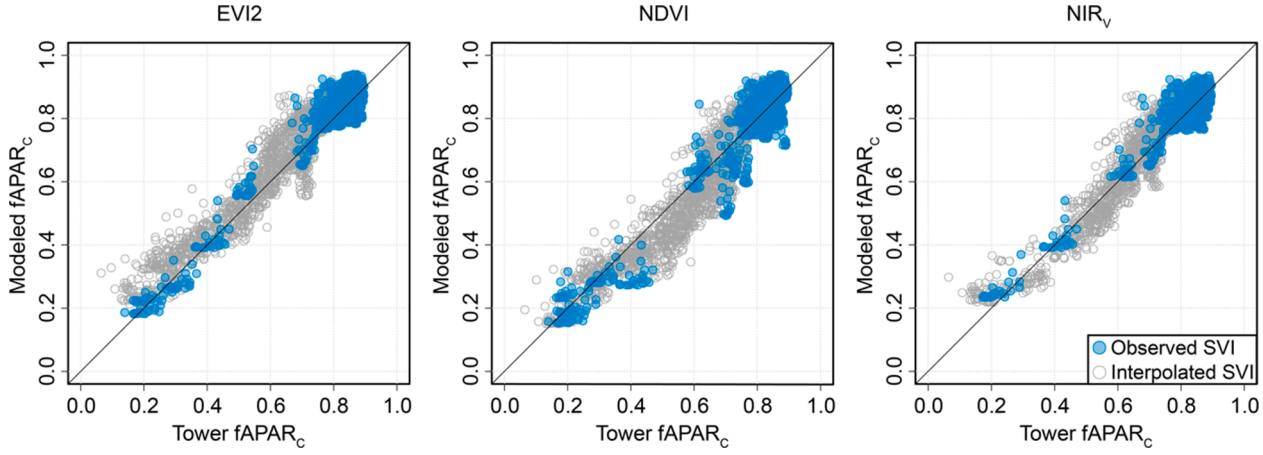

Fig. 11. Modeled 30-minute canopy $fAPAR_C$ estimated from EVI2, NDVI, and NIR_V data using FT04 to estimate half hourly $fAPAR_C$ for observed (filled circles) and daily interpolated SVIs for each (open circles) for 7:00 am to 5:00 pm local time. Note, this figure includes data from all four years.

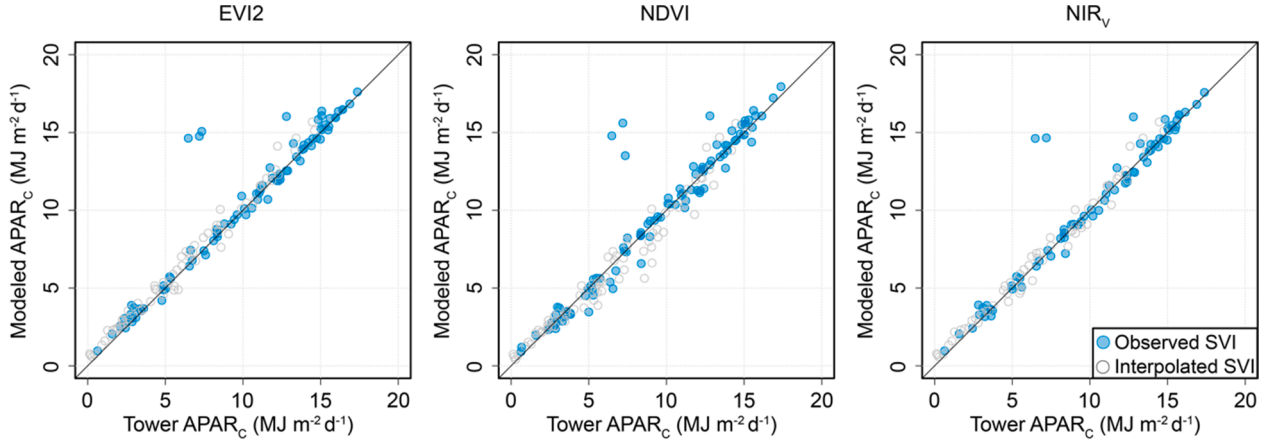

Fig. 12. Daily total PAR absorbed by the canopy ($APAR_C = \Phi_D$) at Harvard Forest estimated from HLS EVI2, NDVI and NIR_V versus Φ_D estimated from tower measurements. Observed SVI indicates Φ_D values estimated from imagery, while interpolated SVI refers to Φ_D values estimated from daily SVI values that were interpolated to daily values from imagery. Note, this figure includes data from all four years.

Table 4
Agreement between observed and modeled values of daily APAR. Bias is defined as Observed – Modeled.

	Observed SVI Only			Observed + Interpolated SVI		
	R^2	RMSE	Bias	R^2	RMSE	Bias
EVI2	0.90	1.57	0.00	0.94	1.22	-0.42
NDVI	0.90	1.50	0.00	0.93	1.24	-0.04
NIR_V	0.91	1.41	0.00	0.95	1.10	-0.24

the dates). In general, all three of the SVIs captured seasonal variation in Φ_D with high accuracy.

4. Discussion

4.1. Estimating LAI phenology from remote sensing

LAI controls a wide array of ecosystem functions related to carbon, water, and energy budgets in terrestrial ecosystems. In temperate deciduous forests, LAI exhibits variation at multiple spatial scales and varies both seasonally and interannually as a function of bioclimatic forcing (e.g., Moon, Seyednasrollah, et al., 2021). In-situ measurements at Harvard Forest demonstrate that during the mid-season period (i.e., after leaf out and prior to senescence) LAI is very stable. Similarly, leaf-level measurements show that foliar spectral reflectance among dominant deciduous tree species at the Harvard Forest is stable during the mid-season (Yang et al., 2016). However, remote sensing-based studies conducted at the Harvard Forest (E. Melaas et al., 2013) and in a Mid-Atlantic temperate forest (Elmore et al., 2012) demonstrate that remotely sensed SVIs exhibit systematic seasonal decrease (aka 'greendown') prior to senescence that is unrelated to changes in LAI and is largely driven by changes in NIR reflectance. Reaves et al. (2018) collected field data designed to explore and explain the source of this pattern. They found that 50% of spatial variation in observed greendown across multiple sites at a mixed oak forest in western Maryland was explained by a combination of species composition and topography. Significantly, Reaves et al (2018) found no consistent seasonal trends in foliar NIR reflectance and no correlation between leaf-level reflectance measurements and satellite-observed greendown patterns. These patterns are consistent with our results. Indeed, our results, in combination with results from Reaves et al. (2018), suggest that the impact of shadowing on surface reflectance will be stronger in forested areas where topography increases the proportional area of shadow in remotely sensed images.

Results from our analysis show that model-based retrievals of LAI estimated from remotely sensed spectral vegetation indices agreed well with ground-based measurements of LAI collected using indirect optical methods (Figs. 7 and 8, Table 1). However, it's important to note that these ground-based estimates include non-trivial uncertainty. Indirect optical LAI measurements, such as the ones used in this work, measure the plant area index (PAI), not LAI. To compute LAI from PAI (Eq. (2)), we estimated the woody fraction (W_f) of the PAI using the method described by Chen et al. (1997). Kucharik et al. (1998) showed that branches can be occluded by leaves, which can lead to over-estimation of W_f. However, Kucharik et al. (1998) also state that the PAI of stems need to be accounted for independent of branches. Further, Yan et al. (2019) found that occlusion of branches is not a major source of error and conclude that the method described by (Chen et al., 1997) provides a practical approach for operational estimation of LAI from PAI measurements. That said, as we previously noted in reference to Fig. 8, the ground-based measurements of LAI (after correcting for woody fraction) appear to saturate around 3.2. It's also worth noting that the transects that where indirect optical measurements of LAI are collected include a modest number of conifer species, which will modestly increase minimum PAI values. Hence, it's possible that the parameterization of W_f that we use for this work modestly over-estimates PAI during the middle of the growing season when PAI tends to be quite stable, leading to modest underestimation of LAI.

Estimation of LAI from remote sensing has been a topic of research for well over three decades and there is a deep literature focused on both theory and applications on this topic (*e.g.* Asrar et al. 1984, Myneni et al. 1995, Knyazikhin et al. 1998b, 1998a, Weiss et al. 1999, Fang et al. 2003, Viña et al. 2011). The goal of this work is not to develop new theory or methods to estimate LAI from remote sensing. Rather, our goal was to test the feasibility of using the relatively simple model described by Baret and Guyot (1991) to estimate seasonal variation in canopy LAI from newly available remote sensing data sets. As part of our analysis, we modified the general approach described Baret and Guyot (1991) to account for variation in canopy properties over the growing season by including seasonal variation in k_{VI} and VI_∞. In doing so, our approach attempts to balance model complexity and realism with practical considerations involved in operational estimation of LAI from remote sensing.

Recent and ongoing changes in climate have shifted the timing of phenophase transition dates in temperate forests (Cleland et al., 2007; Gill et al., 2015; Jeong et al., 2011; Menzel et al., 2006; Piao et al., 2006; A. D. Richardson et al., 2013), which can impact community structure and ecosystem function, including ecosystem primary productivity (Keenan et al., 2014; L. Liu & Zhang, 2020; Piao et al., 2019; A. D. Richardson et al., 2009; Wehr et al., 2016). While previous studies have successfully mapped phenological metrics or LAI from Landsat (J. M. Chen & Cihlar, 1996; E. Melaas et al., 2013; Turner et al., 1999), this study provides a demonstration of 30 m LAI time series retrieval at sub-seasonal time scale, which is made possible by the availability of HLS data. In this context, our results demonstrate the importance of parameterizing seasonal scale variation in environmental properties, especially solar zenith angle, in this process. As we illustrate in Fig. 1, both EVI2 and NIR_V systematically decrease after the summer solstice even though in-situ measurements show that LAI is stable until much later in the growing season. Because leaves are strongly absorptive in the visible wavelengths, canopy reflectance in the HLS red band is unaffected by variation in solar zenith angle. In contrast, NIR reflectance shows strong seasonal co-variation with solar zenith angle, which we parameterized using a first-order model of canopy shadowing. Relative to NDVI, both EVI2 and NIR_V weight NIR reflectance more heavily, and so both indices exhibit seasonal variation that is unrelated to changes in canopy properties that is somewhat less evident in NDVI time series.

A novel aspect of our analysis is that it demonstrates the feasibility of retrieving LAI with sufficient temporal frequency to resolve the phenology of forest canopies at a spatial resolution that captures landscape-scale patterns in phenology. This capability provides substantial information related to spatial variability in canopy LAI that is not detected at coarser spatial resolutions. To illustrate, Fig. 9 shows maps of LAI estimated for two adjacent days at 500 m spatial resolution from the MODIS Collection 6 LAI/fPAR product (K. Yan, Park, Yan, Chen, et al., 2016; K. Yan, Park, Yan, Liu, et al., 2016) and at 30 m resolution estimated from HLS. Inspection of this figure clearly illustrates the additional granularity of landscape-scale information afforded by 30 m HLS imagery relative to MODIS. Because LAI is non-linearly related to both spectral vegetation indices and a wide array of biophysical processes (Friedl et al., 1995; Garrigues et al., 2006; Jin et al., 2007; Y. Xiao et al., 2014), the higher spatial resolution afforded by Landsat and Sentinel 2 imagery has potential to substantially improve not only the spatial representation of seasonal variation in LAI, but also to reduce bias introduced via scaling processes in models that use remotely sensed LAI as inputs.

4.2. Estimating $fAPAR_C$ phenology from remote sensing

We compared two methods for estimating variation in $fAPAR_C$ over the growing season. The first method (BG91) estimates $fAPAR_C$ directly from vegetation indices, while the second method (FT04) estimates

$fAPAR_C$ using remotely sensed estimates of LAI and a first-order model of canopy absorption based on Beer's Law. Our results indicate that both methods were able to accurately estimate seasonal variation in instantaneous $fAPAR_C$ across the growing season. Because FT04 parameterizes the effect of diurnal variation in solar zenith angle on $fAPAR_C$, we used this method to estimate half-hourly $fAPAR_C$ and then aggregated 30-minute values of $fAPAR_C$ with corresponding values of incoming PAR (PAR_i) to estimate daily total PAR absorbed by the canopy (Φ_D).

Significantly, even though FT04 relies on remotely sensed estimates of LAI, when aggregated to daily values derived from 30-minute values of $fAPAR_C$, Φ_D exhibited only modest bias and was relatively insensitive to uncertainty in remotely sensed LAI. This was especially true during the mid-growing season when LAI was high and $fAPAR_C$ was relatively stable. This occurs because the relationship between $fAPAR_C$ and LAI is asymptotic, and for LAI values greater than ~2.0 $fAPAR_C$ was relatively insensitive to changes in LAI Fig. 2. During the spring greenup and fall greendown periods when LAI is lower, however, instantaneous values of $fAPAR_C$ estimated via FT04 were modestly biased, especially for time periods when solar zenith angles were large. Fortunately, because PAR_i is low under these conditions the impact of these systematic errors on Φ_D was relatively minor. However, given the growing importance of the spring and fall phenological sub-periods to changes in net growing season carbon budgets (*e.g.*, Richardson et al. 2009, Keenan et al. 2014), accounting for and correcting the source of this bias is an important issue that needs to be addressed in future work.

It's important to note that our analysis specifically focused on $fAPAR_C$ rather than total fAPAR absorbed by all canopy elements (leaves, branches, and stems; *i.e.,* $fAPAR_T$). Some studies either explicitly or implicitly include woody canopy elements (*i.e.*, branches, trunks) in estimates of fAPAR, while others have showed the importance of distinguishing between photosynthetic and non-photosynthetically active parts of the canopy (Cheng et al., 2014; Gitelson & Gamon, 2015; Hall et al., 1992; Hanan et al., 2002; Viña & Gitelson, 2005; Q. Zhang et al., 2014). Indeed, many indirect methods for estimating LAI do not distinguish between photosynthetically active and non-photosynthetically active canopy elements (discussed in Yan et al. 2019, Rogers et al. 2021). Hence, model-based estimates of $fAPAR_C$ that use LAI values estimated by these indirect methods may not accurately represent fAPAR from leaves (*i.e.*, $fAPAR_C$), which is of primary interest. Because remotely sensed estimates of LAI and fAPAR are most relevant to studies and models focused on ecosystem processes (i.e., carbon, energy and, water budgets), it's important that model-based estimates of fAPAR to distinguish between PAR absorbed by woody elements versus PAR absorbed by leaves in the canopy.

4.3. Relevance to ecosystem models and carbon budgets

The ability to measure and monitor fine-scale spatial heterogeneity in LAI and fAPAR at sub-seasonal to interannual time scales from remote sensing has two important implications for ecosystem monitoring modeling. First, the realism of phenology in ecosystem models is poor (A. D. Richardson et al., 2012), which introduces substantial error and uncertainty in model-based estimates of the current and future carbon budgets of terrestrial ecosystems (M. Chen et al., 2016; E. K. Melaas et al., 2016). Hence, the availability of accurate, fine-scale, and spatially explicit information related to phenology in LAI and fAPAR provides a valuable source of data that can be used to parameterize and refine the representation of phenology in ecosystem models.

Second, multi-year time series of remote sensing provide a valuable source of information related to interannual variability in LAI and fAPAR, and by extension, ecosystem productivity. Because the HLS record is short, the range of interannual variability in phenology at the Harvard Forest for the period we examined is relatively low. Phenological metrics from the 30m Multisource Land Surface Phenology product (Bolton et al., 2020), which is derived from HLS imagery (MSLSP30NA; https://lpdaac.usgs.gov/products/mslsp30nav011), show a total range of 6 days for the date of mid-greenup in spring (DOY 138-144) and 8 days for the date of mid-greendown in fall (DOY 289-297) across the four years included in this study. There is, however, ample evidence that the range of phenological variability at Harvard Forest is substantially greater than 6-8 days in both the spring and fall (Finzi et al., 2020). Further, climate change is likely to increase variability in phenology (e.g., Friedl et al. 2014), and by extension, carbon, energy, and water budgets. Under the assumption that phenological variation in green leaf area is the primary driver of variation in light use efficiency during spring and fall at the Harvard Forest, we estimate that a shift to earlier greenup of 10 days increases GPP by 83.7 g m^{-2} for the period from April 1 to June 21. This translates into an increase in springtime GPP of 22.8% and an increase in annual GPP by 5.6%. Similarly, we estimate that a corresponding shift to later greendown of 10 days increases fall GPP by 18.2 g m^{-2} for the period between the September 21 and December 1 (increases of 10.0% and 1.2% for fall and annual GGP, respectively). These estimates are based on long-term mean data and are thus approximate. However, they are consistent with results from more detailed studies focused on this question (Finzi et al., 2020; A. D. Richardson et al., 2009), and more importantly, they illustrate why improved characterization of sub-seasonal and interannual variation in LAI and fAPAR is important for modeling and quantifying dynamics in the energy, water and carbon budgets in terrestrial ecosystems.

5. Conclusions

In this study, we examined how the relationships between SVIs computed from time series of optical imagery at 30 m spatial resolution and LAI and fAPAR vary over the growing season. Using three different vegetation indices (EVI2, NDVI, and NIR_V) computed from HLS image time series, we estimated LAI time series using the framework originally described by Baret and Guyot (1991), which we adapted to account for seasonal variation in canopy properties and solar zenith angle. We then used the remotely sensed LAI values to estimate 30-minute $fAPAR_C$ and up-scaled these data in combination with 30-minute values of incoming PAR to compute daily values of the total PAR absorbed by the canopy. Our results demonstrate that the relationship between vegetation indices and LAI (and therefore $fAPAR_C$) varies seasonally (primarily because of variation in solar zenith angle), but if this seasonal variation is accounted for, phenological variation in LAI, $fAPAR_C$ and daily APAR can be retrieved using time series of HLS imagery with good accuracy.

Remote sensing has been used for decades to map and monitor LAI and fAPAR. With the launch of Sentinel 2A and 2B by the European Space Agency in 2015 and 2017, respectively, the potential for remote sensing-based monitoring vegetation properties and function has dramatically increased. We can now monitor the phenology of canopy properties at spatial resolutions that are an order of magnitude higher than was previously possible from instruments such as MODIS. Indeed, a variety of recent studies have demonstrated that this is possible at even higher spatial resolution using commercial imagery (Houborg & McCabe, 2018; Moon, Richardson, et al., 2021). Because ecosystems are spatially and temporally heterogeneous and are increasingly subject to disturbance and changes in phenology, the ability to monitor these changes at spatial resolutions that resolve landscape properties provides important new capabilities and opportunities to improve understanding of how ecosystem properties and processes are changing in response to climate change. The results we present here provide an important proof-of-concept regarding both the feasibility of monitoring sub-seasonal variation in vegetation canopy properties, as well as the potential value and utility of mapping these properties at spatial resolutions that capture landscape-scale variation in vegetation in a way that was not previously possible (Figs. 6 and 13).

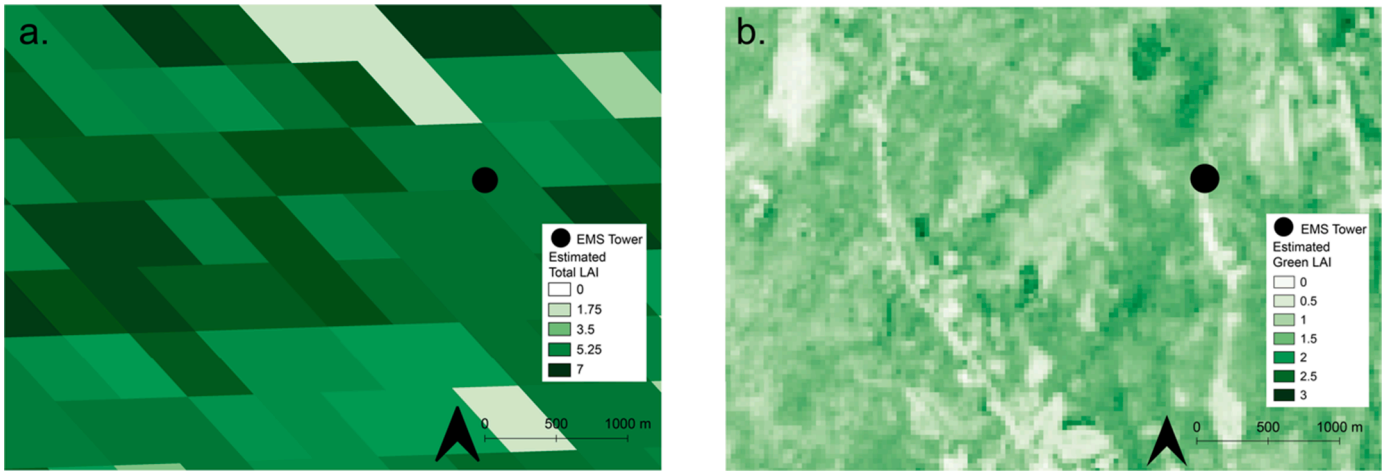

Fig. 13. (a) MODIS LAI data on July 3, 2016, and (b) LAI estimated at 30 m spatial resolution from Landsat data at Harvard Forest for July 4, 2016. Each MODIS pixel includes 238 HLS pixels. Note that the color scale is different in each figure because the MODIS LAI product is systematically higher than LAI values from HLS.

Declaration of Competing Interest

The authors declare that they have no known competing financial interests or personal relationships that could have appeared to influence the work reported in this paper.

Data availability

Data will be made available on request.

Acknowledgements

This work was partly supported by NASA award number 80NSSC18K0334 and NSF award number award 1702627. The field data for this work came from the Biomass Inventories at Harvard Forest EMS tower. Special thanks to Mark VanScoy for on-site maintenance of remote measurement stations and contribution to field data collection as well as many other research assistants who have contributed to the Biomass inventory plot measurements over the years. Tower and plot-level measurements were supported by the AmeriFlux Management Project with funding by the U.S. Department of Energy's Office of Science under Contract No. DE-AC02-05CH11231, and by the National Science Foundation (DEB-1832210) as a component of the Harvard Forest LTER site.

References

Anav, A., Friedlingstein, P., Beer, C., Ciais, P., Harper, A., Jones, C., Murray-Tortarolo, G., Papale, D., Parazoo, N.C., Peylin, P., Piao, S., Sitch, S., Viovy, N., Wiltshire, A., Zhao, M., 2015. Spatiotemporal patterns of terrestrial gross primary production: A review. Rev Geophys 53 (3), 785–818. https://doi.org/10.1002/2015RG000483.

Asner, G.P., 1998. Biophysical and biochemical sources of variability in canopy reflectance. Remote Sens Environ 64 (3), 234–253. https://doi.org/10.1016/S0034-4257(98)00014-5.

Asrar, G., Fuchs, M., Kanemasu, E.T., Hatfield, J.L., 1984. Estimating absorbed photosynthetic radiation and leaf area index from spectral reflectance in wheat1. Agron J 76 (2), 300–306. https://doi.org/10.2134/agronj1984.00021962007600020029x.

Badgley, G., Field, C.B., Berry, J.A., 2017. Canopy near-infrared reflectance and terrestrial photosynthesis. Sci Adv 3 (3), e1602244. https://doi.org/10.1126/sciadv.1602244.

Baret, F., Guyot, G., 1991. Potentials and limits of vegetation indices for LAI and APAR assessment. Remote Sens Environ 35 (2), 161–173. https://doi.org/10.1016/0034-4257(91)90009-U.

Baret, F., Hagolle, O., Geiger, B., Bicheron, P., Miras, B., Huc, M., Berthelot, B., Niño, F., Weiss, M., Samain, O., Roujean, J.L., Leroy, M., 2007. LAI, fAPAR and fCover CYCLOPES global products derived from VEGETATION: Part 1: Principles of the algorithm. Remote Sens Environ 110 (3), 275–286. https://doi.org/10.1016/j.rse.2007.02.018.

Bolton, D.K., Gray, J.M., Melaas, E.K., Moon, M., Eklundh, L., Friedl, M.A., 2020. Continental-scale land surface phenology from harmonized Landsat 8 and Sentinel-2 imagery. Remote Sens Environ 240, 111685. https://doi.org/10.1016/j.rse.2020.111685.

Bonan, G.B., Doney, S.C., 2018. Climate, ecosystems, and planetary futures: The challenge to predict life in Earth system models. Science (6375), 359. https://doi.org/10.1126/science.aam8328.

Breiman, L., 2001. Random Forests. Machine Learning 45 (1), 5–32. https://doi.org/10.1023/A:1010933404324.

Buermann, W., Bikash, P.R., Jung, M., Burn, D.H., Reichstein, M., 2013. Earlier springs decrease peak summer productivity in North American boreal forests. Environ Res Lett 8 (2), 024027. https://doi.org/10.1088/1748-9326/8/2/024027.

Campbell, G.S., Norman, J.M., 1998. The light environment of plant canopies. In: Campbell, G.S., Norman, J.M. (Eds.), An Introduction to Environmental Biophysics. Springer, pp. 247–278. https://doi.org/10.1007/978-1-4612-1626-1_15.

Chen, J.M., 1996. Canopy architecture and Remote Sensing of the fraction of photosynthetically active radiation absorbed by boreal conifer forests. IEEE Trans Geosci Remote Sens 34 (6), 1353–1368. https://doi.org/10.1109/36.544559.

Chen, J.M., Rich, P.M., Gower, S.T., Norman, J.M., Plummer, S., 1997. Leaf area index of boreal forests: Theory, techniques, and measurements. J. Geophys. Res. 102(D24), 29429-29443. doi:10.1029/97JD01107.

Chen, J.M., Cihlar, J., 1996. Retrieving leaf area index of boreal conifer forests using Landsat TM images. Remote Sens Environ 55 (2), 153–162. https://doi.org/10.1016/0034-4257(95)00195-6.

Chen, M., Melaas, E.K., Gray, J.M., Friedl, M.A., Richardson, A.D., 2016. A new seasonal-deciduous spring phenology submodel in the Community Land Model 4.5: Impacts on carbon and water cycling under future climate scenarios. Global Change Biol 22 (11), 3675–3688. https://doi.org/10.1111/gcb.13326.

Cheng, Y.-B., Zhang, Q., Lyapustin, A.I., Wang, Y., Middleton, E.M., 2014. Impacts of light use efficiency and fPAR parameterization on gross primary production modeling. Agric For Meteorol 189–190, 187–197. https://doi.org/10.1016/j.agrformet.2014.01.006.

Claverie, M., Ju, J., Masek, J.G., Dungan, J.L., Vermote, E.F., Roger, J.-C., Skakun, S.V., Justice, C., 2018. The Harmonized Landsat and Sentinel-2 surface reflectance data set. Remote Sens Environ 219, 145–161. https://doi.org/10.1016/j.rse.2018.09.002.

Cleland, E.E., Chuine, I., Menzel, A., Mooney, H.A., Schwartz, M.D., 2007. Shifting plant phenology in response to global change. Trends Ecol Evol 22 (7), 357–365. https://doi.org/10.1016/j.tree.2007.04.003.

Corripio, J., 2003. Vectorial algebra algorithms for calculating terrain parameters from DEMs and solar radiation modeling in mountainous terrain. Int J Geographical Info Sci 17, 1–23. https://doi.org/10.1080/713811744.

Daughtry, C., Vanderbilt, V., Pollara, V., 1982. Variability of Reflectance Measurements with Sensor Altitude and Canopy Type1. Agronomy Journal - AGRON J 74. https://doi.org/10.2134/agronj1982.00021962007400040034x.

de Wit, C.T. (1965). *Photosynthesis of leaf canopies*. Pudoc. http://library.wur.nl/WebQuery/wurpubs/413358.

Dillen, S.Y., de Beeck, M.O., Hufkens, K., Buonanduci, M., Phillips, N.G., 2012. Seasonal patterns of foliar reflectance in relation to photosynthetic capacity and color index in two co-occurring tree species, Quercus rubra and Betula papyrifera. Agric For Meteorol 160, 60–68. https://doi.org/10.1016/j.agrformet.2012.03.001.

D'Odorico, P., Gonsamo, A., Pinty, B., Gobron, N., Coops, N., Mendez, E., Schaepman, M. E., 2014. Intercomparison of fraction of absorbed photosynthetically active radiation products derived from satellite data over Europe. Remote Sens Environ 142, 141–154. https://doi.org/10.1016/j.rse.2013.12.005.

Ellison, A., Munger, W., 2021. Microclimate at Harvard Forest HDW Tower since 2014. Environmental Data Initiative. https://doi.org/10.6073/PASTA/CFC7C9A8CD4D3D1C5DD09E78F59CC48A.

Elmore, A.J., Guinn, S.M., Minsley, B.J., Richardson, A.D., 2012. Landscape controls on the timing of spring, autumn, and growing season length in mid-Atlantic forests. Global Change Biol 18 (2), 656–674. https://doi.org/10.1111/j.1365-2486.2011.02521.x.

Elmore, A.J., Nelson, D.M., Craine, J.M., 2016. Earlier springs are causing reduced nitrogen availability in North American eastern deciduous forests. Nat Plants 2 (10), 10. https://doi.org/10.1038/nplants.2016.133.

Fang, H., Liang, S., Kuusk, A., 2003. Retrieving leaf area index using a genetic algorithm with a canopy radiative transfer model. Remote Sens Environ 85 (3), 257–270. https://doi.org/10.1016/S0034-4257(03)00005-1.

Fensholt, R., Sandholt, I., Rasmussen, M., 2004. Evaluation of MODIS LAI, fAPAR and the relation between fAPAR and NDVI in a semi-arid environment using in situ measurements. Remote Sens Environ 91, 490–507. https://doi.org/10.1016/j.rse.2004.04.009.

Finzi, A.C., Giasson, M.-A., Barker Plotkin, A.A., Aber, J.D., Boose, E.R., Davidson, E.A., Dietze, M.C., Ellison, A.M., Frey, S.D., Goldman, E., Keenan, T.F., Melillo, J.M., Munger, J.W., Nadelhoffer, K.J., Ollinger, S.V., Orwig, D.A., Pederson, N., Richardson, A.D., Savage, K., Foster, D.R., 2020. Carbon budget of the harvard forest long-term ecological research site: pattern, process, and response to global change. Ecological Monographs 90 (4), e01423. https://doi.org/10.1002/ecm.1423.

Friedl, M.A., Davis, F.W., Michaelsen, J., Moritz, M.A., 1995. Scaling and uncertainty in the relationship between the NDVI and land surface biophysical variables: An analysis using a scene simulation model and data from FIFE. Remote Sens Environ 54 (3), 233–246. https://doi.org/10.1016/0034-4257(95)00156-5.

Friedl, M.A., Gray, J.M., Melaas, E.K., Richardson, A.D., Hufkens, K., Keenan, T.F., Bailey, A., O'Keefe, J., 2014. A tale of two springs: Using recent climate anomalies to characterize the sensitivity of temperate forest phenology to climate change. Environ Res Lett 9 (5), 054006. https://doi.org/10.1088/1748-9326/9/5/054006.

Friedlingstein, P., 2015. Carbon cycle feedbacks and future climate change. Philos Trans R Soc, A 373 (2054), 20140421. https://doi.org/10.1098/rsta.2014.0421.

Garrigues, S., Allard, D., Baret, F., Weiss, M., 2006. Influence of landscape spatial heterogeneity on the non-linear estimation of leaf area index from moderate spatial resolution remote sensing data. Remote Sens Environ 105 (4), 286–298. https://doi.org/10.1016/j.rse.2006.07.013.

Gill, A.L., Gallinat, A.S., Sanders-DeMott, R., Rigden, A.J., Short Gianotti, D.J., Mantooth, J.A., Templer, P.H., 2015. Changes in autumn senescence in northern hemisphere deciduous trees: A meta-analysis of autumn phenology studies. Ann Bot 116 (6), 875–888. https://doi.org/10.1093/aob/mcv055.

Gitelson, A.A., Gamon, J.A., 2015. The need for a common basis for defining light-use efficiency: Implications for productivity estimation. Remote Sens Environ 156, 196–201. https://doi.org/10.1016/j.rse.2014.09.017.

Gitelson, A.A., Gritz, Y., Merzlyak, M.N., 2003. Relationships between leaf chlorophyll content and spectral reflectance and algorithms for non-destructive chlorophyll assessment in higher plant leaves. J Plant Physiol 160 (3), 271–282. https://doi.org/10.1078/0176-1617-00887.

Goward, S.N., Huemmrich, K.F., 1992. Vegetation canopy PAR absorptance and the normalized difference vegetation index: An assessment using the SAIL model. Remote Sens Environ 39 (2), 119–140. https://doi.org/10.1016/0034-4257(92)90131-3.

Hall, F.G., Huemmrich, K.F., Goetz, S.J., Sellers, P.J., Nickeson, J.E., 1992. Satellite remote sensing of surface energy balance: Success, failures, and unresolved issues in FIFE. J Geophy Res 97 (D17), 19061–19089. https://doi.org/10.1029/92JD02189.

Hanan, N.P., Burba, G., Verma, S.B., Berry, J.A., Suyker, A., Walter-Shea, E.A., 2002. Inversion of net ecosystem CO2 flux measurements for estimation of canopy PAR absorption. Global Change Biol 8 (6), 563–574. https://doi.org/10.1046/j.1365-2486.2002.00488.x.

He, L., Wood, J.D., Sun, Y., Magney, T., Dutta, D., Köhler, P., Zhang, Y., Yin, Y., Frankenberg, C., 2020. Tracking seasonal and interannual variability in photosynthetic downregulation in response to water stress at a temperate deciduous forest. J Geophy Res 125 (8), e2018JG005002. https://doi.org/10.1029/2018JG005002.

Hipps, L.E., 1983. Assessing the interception of photosynthetically active radiation in winter wheat. Agric Meteorol 28 (3), 253–259.

Houborg, R., McCabe, M.F., 2018. Daily Retrieval of NDVI and LAI at 3 m Resolution via the Fusion of CubeSat, Landsat, and MODIS Data. Remote Sens 10 (6), 6. https://doi.org/10.3390/rs10060890.

Jenkins, J.P., Richardson, A.D., Braswell, B.H., Ollinger, S.V., Hollinger, D.Y., Smith, M.-L., 2007. Refining light-use efficiency calculations for a deciduous forest canopy using simultaneous tower-based carbon flux and radiometric measurements. Agric For Meteorol 143 (1), 64–79. https://doi.org/10.1016/j.agrformet.2006.11.008.

Jeong, S.-J., Ho, C.-H., Gim, H.-J., Brown, M.E., 2011. Phenology shifts at start vs. End of growing season in temperate vegetation over the Northern Hemisphere for the period 1982–2008. Global Change Biol 17 (7), 2385–2399. https://doi.org/10.1111/j.1365-2486.2011.02397.x.

Jiang, Z., Huete, A.R., Didan, K., Miura, T., 2008. Development of a two-band enhanced vegetation index without a blue band. Remote Sens Environ 112 (10), 3833–3845. https://doi.org/10.1016/j.rse.2008.06.006.

Jin, Z., Tian, Q., Chen, J.M., Chen, M., 2007. Spatial scaling between leaf area index maps of different resolutions. J Environ Manage 85 (3), 628–637. https://doi.org/10.1016/j.jenvman.2006.08.016.

Jonsson, P., Eklundh, L., 2002. Seasonality extraction by function fitting to time-series of satellite sensor data. IEEE Trans Geosci Remote Sens 40 (8), 1824–1832. https://doi.org/10.1109/TGRS.2002.802519.

Keenan, T.F., Gray, J., Friedl, M.A., Toomey, M., Bohrer, G., Hollinger, D.Y., Munger, J.W., O'Keefe, J., Schmid, H.P., Wing, I.S., Yang, B., Richardson, A.D., 2014. Net carbon uptake has increased through warming-induced changes in temperate forest phenology. Nature Climate Change 4 (7), 598–604. https://doi.org/10.1038/nclimate2253.

Knyazikhin, Y., Martonchik, J.V., Diner, D.J., Myneni, R.B., Verstraete, M., Pinty, B., Gobron, N., 1998. Estimation of vegetation canopy leaf area index and fraction of absorbed photosynthetically active radiation from atmosphere-corrected MISR data. J Geophy Res 103 (D24), 32239–32256. https://doi.org/10.1029/98JD02461.

Knyazikhin, Y., Martonchik, J.V., Myneni, R.B., Diner, D.J., Running, S.W., 1998. Synergistic algorithm for estimating vegetation canopy leaf area index and fraction of absorbed photosynthetically active radiation from MODIS and MISR data. J Geophy Res 103 (D24), 32257–32275. https://doi.org/10.1029/98JD02462.

Kucharik, C.J., Norman, J.M., Gower, S.T., 1998. Measurements of branch area and adjusting leaf area index indirect measurements. Agric For Meteorol 91 (1), 69–88. https://doi.org/10.1016/S0168-1923(98)00064-1.

Le Quéré, C., Andrew, R.M., Friedlingstein, P., Sitch, S., Hauck, J., Pongratz, J., Pickers, P.A., Korsbakken, J.I., Peters, G.P., Canadell, J.G., Arneth, A., Arora, V.K., Barbero, L., Bastos, A., Bopp, L., Chevallier, F., Chini, L.P., Ciais, P., Doney, S.C., Zheng, B., 2018. Global Carbon Budget 2018. Earth System Sci Data 10 (4), 2141–2194. https://doi.org/10.5194/essd-10-2141-2018.

Li, W., Fang, H., 2015. Estimation of direct, diffuse, and total FPARs from Landsat surface reflectance data and ground-based estimates over six FLUXNET sites. J Geophys Res 120 (1), 96–112. https://doi.org/10.1002/2014JG002754.

Liu, D., Piao, S., Wang, T., Wang, X., Wang, X., Ding, J., Ciais, P., Peñuelas, J., Janssens, I., 2018. Decelerating autumn CO2 release with warming induced by attenuated temperature dependence of respiration in northern ecosystems. Geophys Res Lett 45 (11), 5562–5571. https://doi.org/10.1029/2018GL077447.

Liu, L., Zhang, X., 2020. Effects of temperature variability and extremes on spring phenology across the contiguous United States from 1982 to 2016. Sci Rep 10 (1), 17952. https://doi.org/10.1038/s41598-020-74804-4.

Melaas, E., Friedl, M., Zhu, Z., 2013. Detecting interannual variation in deciduous broadleaf forest phenology using Landsat TM/ETM plus data. Remote Sens Environ 132, 176–185. https://doi.org/10.1016/j.rse.2013.01.011.

Melaas, E.K., Friedl, M.A., Richardson, A.D., 2016. Multiscale modeling of spring phenology across Deciduous Forests in the Eastern United States. Global Change Biol 22 (2), 792–805. https://doi.org/10.1111/gcb.13122.

Menzel, A., Sparks, T.H., Estrella, N., Koch, E., Aasa, A., Ahas, R., Alm-Kübler, K., Bissolli, P., Braslavská, O., Briede, A., Chmielewski, F.M., Crepinsek, Z., Curnel, Y., Dahl, Å., Defila, C., Donnelly, A., Filella, Y., Jatczak, K., Måge, F., Zust, A., 2006. European phenological response to climate change matches the warming pattern. Global Change Biol 12 (10), 1969–1976. https://doi.org/10.1111/j.1365-2486.2006.01193.x.

Moon, M., Richardson, A.D., Friedl, M.A., 2021. Multiscale assessment of land surface phenology from harmonized Landsat 8 and Sentinel-2, PlanetScope, and PhenoCam imagery. Remote Sens Environ 266, 112716. https://doi.org/10.1016/j.rse.2021.112716.

Moon, M., Seyednasrollah, B., Richardson, A.D., Friedl, M.A., 2021. Using time series of MODIS land surface phenology to model temperature and photoperiod controls on spring greenup in North American deciduous forests. Remote Sens Environ 260, 112466. https://doi.org/10.1016/j.rse.2021.112466.

Munger, W., Wofsy, S., 2022. Canopy-Atmosphere Exchange of Carbon, Water and Energy at Harvard Forest EMS Tower since 1991. Environmental Data Initiative. https://doi.org/10.6073/PASTA/87DE3421E155B05FD166B17D17C73C6D.

Myneni, R.B., Hall, F.G., Sellers, P.J., Marshak, A.L., 1995. The interpretation of spectral vegetation indexes. IEEE Trans Geosci Remote Sens 33 (2), 481–486. https://doi.org/10.1109/36.377948.

Myneni, R.B., Williams, D.L., 1994. On the relationship between FAPAR and NDVI. Remote Sens Environ 49 (3), 200–211. https://doi.org/10.1016/0034-4257(94)90016-7.

Penuelas, J., Frederic, B., Filella, I., 1995. Semi-empirical indices to assess carotenoids/chlorophyll-a ratio from leaf spectral reflectance. Photosynthetica 31, 221–230.

Piao, S., Fang, J., Zhou, L., Ciais, P., Zhu, B., 2006. Variations in satellite-derived phenology in China's temperate vegetation. Global Change Biol 12 (4), 672–685. https://doi.org/10.1111/j.1365-2486.2006.01123.x.

Piao, S., Liu, Q., Chen, A., Janssens, I.A., Fu, Y., Dai, J., Liu, L., Lian, X., Shen, M., Zhu, X., 2019. Plant phenology and global climate change: Current progresses and challenges. Global Change Biol 25 (6), 1922–1940. https://doi.org/10.1111/gcb.14619.

Raabe, K., Pisek, J., Sonnentag, O., Annuk, K., 2015. Variations of leaf inclination angle distribution with height over the growing season and light exposure for eight broadleaf tree species. Agric For Meteorol 214–215, 2–11. https://doi.org/10.1016/j.agrformet.2015.07.008.

Reaves, V.C., Elmore, A.J., Nelson, D.M., McNeil, B.E., 2018. Drivers of spatial variability in greendown within an oak-hickory forest landscape. Remote Sens Environ 210, 422–433. https://doi.org/10.1016/j.rse.2018.03.027.

Richardson, A.D., Anderson, R.S., Arain, M.A., Barr, A.G., Bohrer, G., Chen, G., Chen, J. M., Ciais, P., Davis, K.J., Desai, A.R., Dietze, M.C., Dragoni, D., Garrity, S.R., Gough, C.M., Grant, R., Hollinger, D.Y., Margolis, H.A., McCaughey, H., Migliavacca, M., Xue, Y., 2012. Terrestrial biosphere models need better representation of vegetation phenology: Results from the North American Carbon Program Site Synthesis. Global Change Biol 18 (2), 566–584. https://doi.org/10.1111/j.1365-2486.2011.02562.x.

Richardson, A.D., Andy Black, T., Ciais, P., Delbart, N., Friedl, M.A., Gobron, N., Hollinger, D.Y., Kutsch, W.L., Longdoz, B., Luyssaert, S., Migliavacca, M., Montagnani, L., William Munger, J., Moors, E., Piao, S., Rebmann, C., Reichstein, M., Saigusa, N., Tomelleri, E., Varlagin, A., 2010. Influence of spring and autumn phenological transitions on forest ecosystem productivity. Philos Trans Royal Soc B 365 (1555), 3227–3246. https://doi.org/10.1098/rstb.2010.0102.

Richardson, A.D., Hollinger, D.Y., Dail, D.B., Lee, J.T., Munger, J.W., O'keefe, J., 2009. Influence of spring phenology on seasonal and annual carbon balance in two contrasting New England forests. Tree Physiol 29 (3), 321–331. https://doi.org/10.1093/treephys/tpn040.

Richardson, A.D., Keenan, T.F., Migliavacca, M., Ryu, Y., Sonnentag, O., Toomey, M., 2013. Climate change, phenology, and phenological control of vegetation feedbacks to the climate system. Agric For Meteorol 169, 156–173. https://doi.org/10.1016/j.agrformet.2012.09.012.

Richardson, A., Hollinger, D., 2019. AmeriFlux BASE US-Bar Bartlett Experimental Forest, Ver. 5-5. AmeriFlux AMP. https://doi.org/10.17190/AMF/1246030.

Rogers, C., Chen, J.M., Croft, H., Gonsamo, A., Luo, X., Bartlett, P., Staebler, R.M., 2021. Daily leaf area index from photosynthetically active radiation for long term records of canopy structure and leaf phenology. Agric For Meteorol 304–305, 108407. https://doi.org/10.1016/j.agrformet.2021.108407.

Russell, G., Jarvis, P.G., Monteith, J.L., 1989. Absorption of radiation by canopies and stand growth. In: Marshall, B., Russell, G., Jarvis, P.G. (Eds.), Plant Canopies: Their Growth, Form and Function. Cambridge University Press, pp. 21–40. https://doi.org/10.1017/CBO9780511752308.003.

Ryu, Y., Verfaillie, J., Macfarlane, C., Kobayashi, H., Sonnentag, O., Vargas, R., Ma, S., Baldocchi, D.D., 2012. Continuous observation of tree leaf area index at ecosystem scale using upward-pointing digital cameras. Remote Sens Environ 126, 116–125. https://doi.org/10.1016/j.rse.2012.08.027.

Schimel, D., Pavlick, R., Fisher, J.B., Asner, G.P., Saatchi, S., Townsend, P., Miller, C., Frankenberg, C., Hibbard, K., Cox, P., 2015. Observing terrestrial ecosystems and the carbon cycle from space. Global Change Biol 21 (5), 1762–1776. https://doi.org/10.1111/gcb.12822.

Sellers, P.J., 1985. Canopy reflectance, photosynthesis and transpiration. Int J Remote Sens 6 (8), 1335–1372. https://doi.org/10.1080/01431168508948283.

Toda, M., Richardson, A.D., 2018. Estimation of plant area index and phenological transition dates from digital repeat photography and radiometric approaches in a hardwood forest in the Northeastern United States. Agric For Meteorol 249, 457–466. https://doi.org/10.1016/j.agrformet.2017.09.004.

Tucker, C.J., 1979. Red and photographic infrared linear combinations for monitoring vegetation. Remote Sens Environ 8 (2), 127–150. https://doi.org/10.1016/0034-4257(79)90013-0.

Turner, D.P., Cohen, W.B., Kennedy, R.E., Fassnacht, K.S., Briggs, J.M., 1999. Relationships between Leaf Area Index and Landsat TM Spectral Vegetation Indices across Three Temperate Zone Sites. Remote Sens Environ 70 (1), 52–68. https://doi.org/10.1016/S0034-4257(99)00057-7.

Verhoef, W., 1984. Light scattering by leaf layers with application to canopy reflectance modeling: The SAIL model. Remote Sens Environ 16 (2), 125–141. https://doi.org/10.1016/0034-4257(84)90057-9.

Viña, A., Gitelson, A.A., 2005. New developments in the remote estimation of the fraction of absorbed photosynthetically active radiation in crops. Geophys Res Lett (17), 32. https://doi.org/10.1029/2005GL023647.

Viña, A., Gitelson, A.A., Nguy-Robertson, A.L., Peng, Y., 2011. Comparison of different vegetation indices for the remote assessment of green leaf area index of crops. Remote Sens Environ 115 (12), 3468–3478. https://doi.org/10.1016/j.rse.2011.08.010.

Wehr, R., Munger, J.W., McManus, J.B., Nelson, D.D., Zahniser, M.S., Davidson, E.A., Wofsy, S.C., Saleska, S.R., 2016. Seasonality of temperate forest photosynthesis and daytime respiration. Nature 534 (7609), 680–683. https://doi.org/10.1038/nature17966.

Weiss, M., Baret, F., Leroy, M., BéGué, AS., Hautecoeur, O., Santer, R., 1999. Hemispherical reflectance and albedo estimates from the accumulation of across-track sun-synchronous satellite data. J Geophys Res 104, 22,221. https://doi.org/10.1029/1999JD900415. -22,232.

Wolf, J., West, T.O., Page, Y.L., Kyle, G.P., Zhang, X., Collatz, G.J., Imhoff, M.L., 2015. Biogenic carbon fluxes from global agricultural production and consumption. Global Biogeochem Cycles 29 (10), 1617–1639. https://doi.org/10.1002/2015GB005119.

Xiao, J., Chevallier, F., Gomez, C., Guanter, L., Hicke, J.A., Huete, A.R., Ichii, K., Ni, W., Pang, Y., Rahman, A.F., Sun, G., Yuan, W., Zhang, L., Zhang, X., 2019. Remote sensing of the terrestrial carbon cycle: A review of advances over 50 years. Remote Sens Environ 233, 111383. https://doi.org/10.1016/j.rse.2019.111383.

Xiao, Y., Zhao, W., Zhou, D., Gong, H., 2014. Sensitivity analysis of vegetation reflectance to biochemical and biophysical variables at leaf, canopy, and regional scales. IEEE Trans Geosci Remote Sens 52 (7), 4014–4024. https://doi.org/10.1109/TGRS.2013.2278838.

Yan, G., Hu, R., Luo, J., Weiss, M., Jiang, H., Mu, X., Xie, D., Zhang, W., 2019. Review of indirect optical measurements of leaf area index: Recent advances, challenges, and perspectives. Agric For Meteorol 265, 390–411. https://doi.org/10.1016/j.agrformet.2018.11.033.

Yan, K., Park, T., Yan, G., Chen, C., Yang, B., Liu, Z., Nemani, R.R., Knyazikhin, Y., Myneni, R.B., 2016. Evaluation of MODIS LAI/FPAR Product Collection 6. Part 1: Consistency and Improvements. Remote Sens 8 (5), 5. https://doi.org/10.3390/rs8050359.

Yan, K., Park, T., Yan, G., Liu, Z., Yang, B., Chen, C., Nemani, R.R., Knyazikhin, Y., Myneni, R.B., 2016. Evaluation of MODIS LAI/FPAR Product Collection 6. Part 2: Validation and Intercomparison. Remote Sens 8 (6), 6. https://doi.org/10.3390/rs8060460.

Yang, X., Tang, J., Mustard, J.F., Wu, J., Zhao, K., Serbin, S., Lee, J.-E., 2016. Seasonal variability of multiple leaf traits captured by leaf spectroscopy at two temperate deciduous forests. Remote Sens Environ 179, 1–12. https://doi.org/10.1016/j.rse.2016.03.026.

Zani, D., Crowther, T.W., Mo, L., Renner, S.S., Zohner, C.M., 2020. Increased growing-season productivity drives earlier autumn leaf senescence in temperate trees. Science 370 (6520), 1066–1071. https://doi.org/10.1126/science.abd8911.

Zhang, Q., Cheng, Y.-B., Lyapustin, A.I., Wang, Y., Gao, F., Suyker, A., Verma, S., Middleton, E.M., 2014. Estimation of crop gross primary production (GPP): FAPARchl versus MOD15A2 FPAR. Remote Sens Environ 153, 1–6. https://doi.org/10.1016/j.rse.2014.07.012.

Zhang, X., Friedl, M.A., Schaaf, C.B., Strahler, A.H., Hodges, J.C.F., Gao, F., Reed, B.C., Huete, A., 2003. Monitoring vegetation phenology using MODIS. Remote Sens Environ 84 (3), 471–475. https://doi.org/10.1016/S0034-4257(02)00135-9.